ACS Chemical Neuroscience

Research Article

pubs.acs.org/chemneuro

Superoxide Dismutase 1 (SOD1)-Derived Peptide Inhibits Amyloid Aggregation of Familial Amyotrophic Lateral Sclerosis SOD1 Mutants

Victor Banerjee,[†,∥] Tom Shani,[‡] Bella Katzman,[§] Maria Vyazmensky,[§,∥] Niv Papo,[†,∥] Adrian Israelson,[‡] and Stanislav Engel*[,§,∥]

[†]Department of Biotechnology Engineering, Faculty of Engineering, Ben-Gurion University of the Negev, Beer-Sheva 8410501, Israel

[‡]Department of Physiology and Cell Biology, Faculty of Health Sciences, Ben-Gurion University of the Negev, Beer-Sheva 8410501, Israel

[§]Department of Clinical Biochemistry and Pharmacology, Faculty of Health Sciences, Ben-Gurion University of the Negev, Beer-Sheva 8410501, Israel

[∥]National Institute for Biotechnology in the Negev, Ben-Gurion University of the Negev, Beer-Sheva 8410501, Israel

Supporting Information

ABSTRACT: Amyotrophic lateral sclerosis (ALS) is a neurodegenerative disorder that leads to the death of the upper and lower motor neurons. Superoxide dismutase 1 (SOD1) is an ALS pathogenic protein, whose misfolding results in the formation of amyloid aggregates. The mechanism underlying SOD1 pathogenesis in ALS remains obscure, but one possible mechanism involves gain-of-interaction, in which the misfolded soluble SOD1 forms abnormal protein−protein interactions (PPIs) with various cellular proteins, including with other SOD1 molecules, thereby interfering with their function. The structural basis of this gain-of-interaction mechanism is unknown. Here, we characterized the backbone dynamics landscape of misfolded SOD1 to pinpoint surface areas predisposed to aberrant PPIs. This analysis enabled us to formulate a working hypothesis for the mechanism of the gain-of-function of misfolded SOD1, according to which an abnormal PPI potential results from the increased mobility of the SOD1 surface backbone. Guided by the backbone dynamics landscape, we have identified a SOD1-derived peptide that can bind SOD1 proteins and divert the typical amyloid aggregation of ALS-related SOD1 mutants toward a potentially less toxic amorphous aggregation pathway.

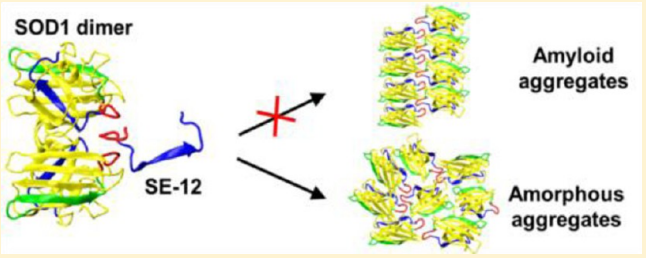

KEYWORDS: *Amyotrophic lateral sclerosis (ALS), superoxide dismutase 1 (SOD1), amyloid aggregation, steered molecular dynamics (SMD), stability patches, gain-of-function*

Proteopathies constitute a broad range of debilitating diseases that result from protein misfolding and aggregation.[1] In these diseases, mutations or environmental stresses often induce a sequential transformation of the structure of certain proteins that, thereby, either lose their original function or gain a new, noxious one. Whereas the loss-of-function mechanisms have been relatively well characterized, the intermediate toxic species along the structural transformation pathway in gain-of-function mechanisms are yet to be identified.[2]

A gain-of-function mechanism appears to be involved in the pathogenesis of certain types of amyotrophic lateral sclerosis (ALS), a rapidly progressing neurodegenerative proteopathy that leads to the gradual degeneration and death of motor neurons.[3,4] Approximately 10% of ALS cases are inherited ("familial"), and more than 100 ALS-related genes have been identified.[5] Of all familial cases of ALS, approximately 20% are known to result from mutations in the gene that encodes the enzyme copper−zinc superoxide dismutase 1 (SOD1), a ubiquitous 32 kDa homodimeric protein that is critical for cellular defense against reactive oxygen species.[6] To date, more than 150 mutations, termed fALS mutations, have been identified in SOD1 and were described as causing ALS in a dominant fashion.[7,8] In addition, exposure of the wild-type SOD1 ($SOD1^{WT}$) to cell- or tissue-specific cellular stress has been suggested to underlie a significant part of the sporadic cases of ALS.[9,10] Phenotypically, SOD1-related ALS is manifested in the accumulation of amyloid aggregates of misfolded SOD1.[11] However, the pathogenesis of SOD1-related ALS is increasingly attributed to noxious gain-of-function activity of the soluble misfolded SOD1 species,[12−15] which exert several downstream pathophysiological effects, including impaired mitochondrial metabolism, axonal degeneration, axonal transport failure, excitotoxicity, proteasomal disruption, endoplasmic reticulum stress, and more.[4] The

Received: July 31, 2016
Accepted: August 19, 2016
Published: August 19, 2016

DOI: 10.1021/acschemneuro.6b00227
ACS Chem. Neurosci. 2016, 7, 1595−1606

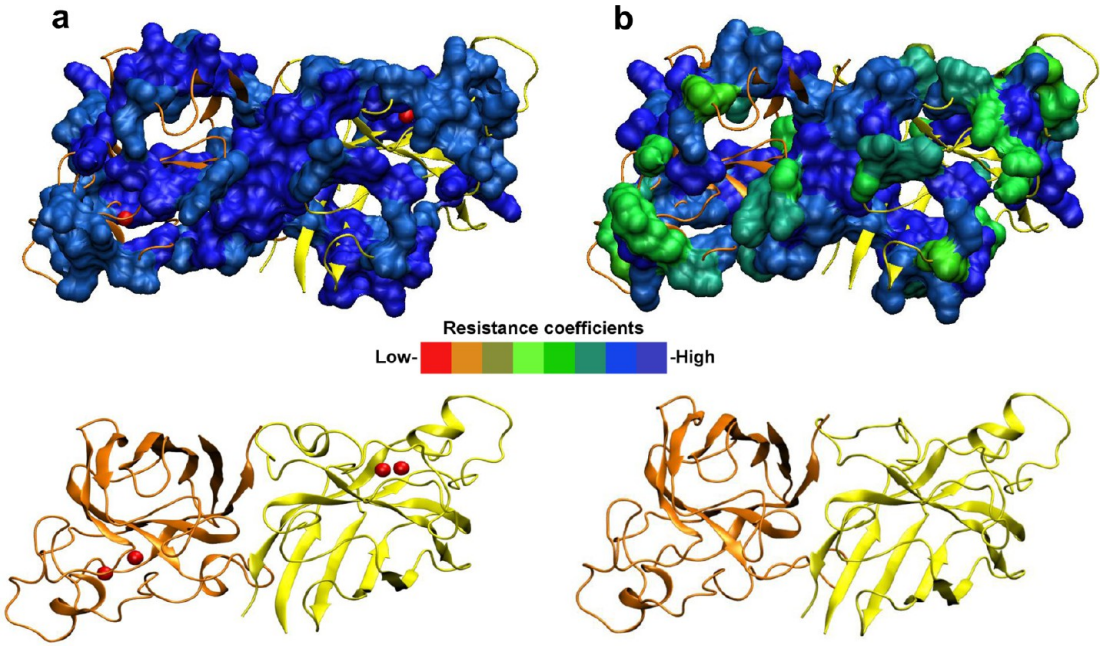

Figure 1. Misfolding causes changes in the SOD1 surface backbone dynamics properties. (a) A WT holo-SOD1 homodimer (PDB 1HL5). Only static surface-exposed residues ("stability patches") are shown in the surface representation and are colored according to their corresponding resistance coefficients (blue designates static residues). (b) A reduced apo-SOD1 homodimer (PDB 2GBU). The same residues as in panel a are shown, colored according to their corresponding resistance coefficients. The size of the original (holo-SOD1) stability patches (i.e., the number of static residues, in blue) was decreased by 36% in apo-SOD1 (recolored in green).

identity of the soluble misfolded SOD1 species and the mechanisms underlying their toxicity remain obscure.

fALS mutations are distributed with no apparent pattern throughout the SOD1 sequence and may cause SOD1 misfolding by promoting SOD1 demetalation (i.e., the formation of apo-SOD1) and reducing the stabilizing *intra-subunit* disulfide bond, thereby lowering the stability of SOD1 monomers or destabilizing the dimer interface.[16−18] fALS mutations may also interfere with SOD1 binding to the copper chaperone for SOD1 (CCS), which normally recognizes newly synthesized SOD1 and activates it by facilitating the insertion of catalytic copper and oxidizing the disulfide bonds.[19] Thus, in the course of structural transformation, the global stability of SOD1 progressively decreases, such that the misfolded SOD1 eventually precipitates to form amyloid aggregates. The noxious species that arise during this process are yet unidentified, but the soluble monomers and the low-molecular weight SOD1 oligomers that form along the aggregation pathway appear to be particularly attractive candidates.[20,21]

SOD1 toxicity may result from the ability of misfolded SOD1 to form aberrant interactions with numerous cellular proteins and interfere with their normal functions.[22−30] Misfolded SOD1 mutants ($SOD1^{MUT}$) can interact with structurally diverse proteins, suggesting that their surface contains conformationally adaptive interaction hot spot(s).[31,32] A similar mechanism may also underlie the abnormal interactions of misfolded SOD1 proteins among themselves, which leads to amyloid aggregation, a phenotypic hallmark of ALS pathology. Thus, the gain-of-interaction of misfolded SOD1 appears to indicate that, upon misfolding, certain elements of the SOD1 surface acquire structural and functional similarities to protein surfaces involved in the formation of interfaces in protein complexes. Such a scenario, of "hot spots on the loose", may inflict substantial cell damage by perturbing the proper homeostasis of protein−protein interactions (PPIs) because SOD1 is a very abundant (∼1% of the total protein in human nervous tissue[33]) and ubiquitous (extracellular, cytoplasmic, nuclear, and intramitochondrial) protein. In ALS, the misfolded SOD1 may interfere with the activity of one or more proteins that are predominantly expressed in motor neurons or that play a vital role in the homeostasis of these cells.

We previously hypothesized that backbone dynamics plays an important role in defining the functional characteristics of protein surfaces, particularly their potential to participate in PPIs.[31,32,34] By using a computational analysis based on a steered molecular dynamics (SMD) simulation, we demonstrated that interfaces in protein complexes are characterized by the presence of so-called "stability patches", clusters of static residues surrounded by areas of moderate to high backbone mobility. We concluded that the stability patches on the interface facilitate protein complex formation by moderating the conformational entropy of the unbound state, diminishing enthalpy−entropy compensation upon binding, and augmenting the favorable entropy of desolvation. In complexes with broad selectivity, in which a protein has multiple and structurally diverse partners, the stability patches may nucleate a directional process of structural adaptation at the interface (i.e., induced fit). Such a conformational adaptation is essential to ensure that the available interaction potential is efficiently utilized to convert the initial, weak complex into a stable one. This conversion process, however, is possible only if the stability patch on the interface is surrounded by regions whose backbone mobility is sufficiently high.

Here, we extended the application of SMD analysis to study the phenomenon of SOD1 proteopathy in ALS. By considering the backbone dynamics as an important factor shaping the PPI potential of protein surfaces, we studied the SOD1 noxious transformation by analyzing the changes in the SOD surface

DOI: 10.1021/acschemneuro.6b00227
ACS Chem. Neurosci. 2016, 7, 1595−1606

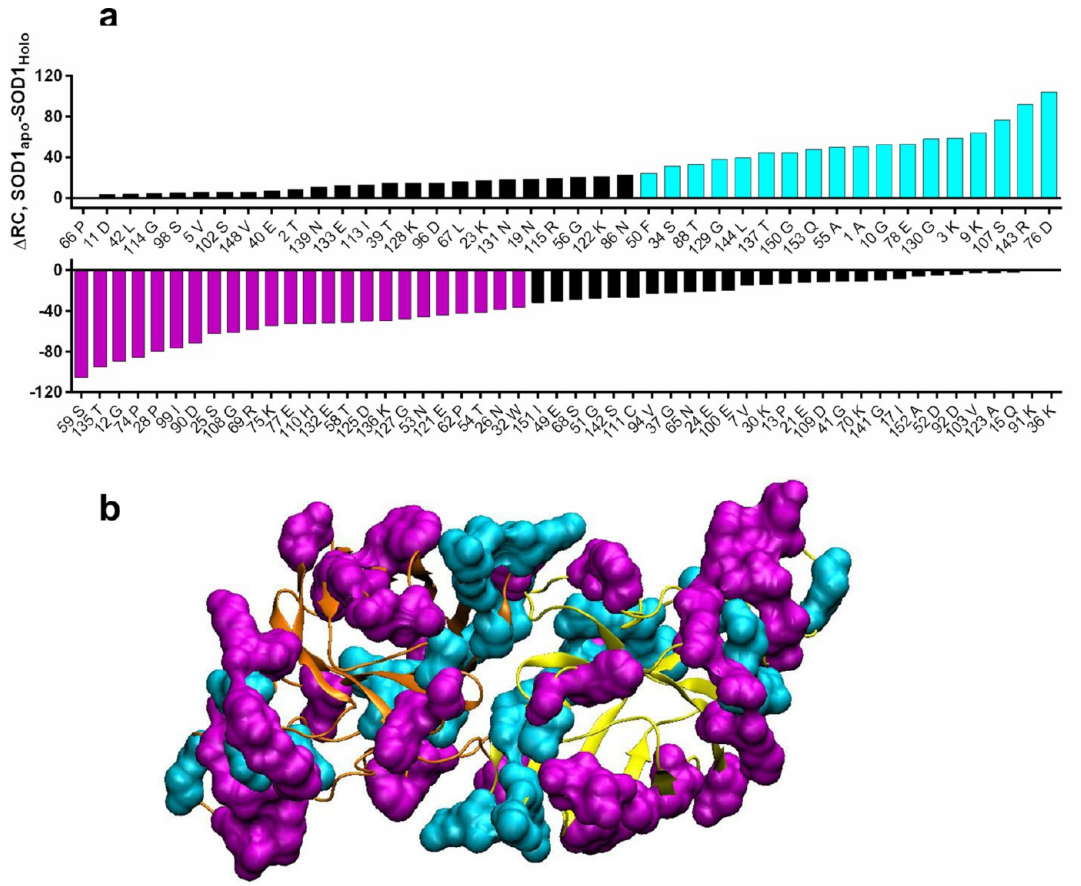

Figure 2. Misfolding reshapes the SOD1 "stability patch" landscape. Resistance coefficients (RC) of surface-exposed residues in the holo-SOD1 and apo-SOD1 structures were calculated by using SMD analysis, as described in the Methods section. (a) ΔRC was calculated as the difference between the RC of the residue in apo-SOD1 and in holo-SOD1. Residues whose mobility changed significantly (>33 pN/Å) in the transition from the holo-SOD1 to the reduced apo-SOD1 are colored in magenta (increased mobility) or cyan (decreased mobility). (b) Structure of the apo-SOD1 homodimer (PDB 2GBU). Residues whose mobility changed significantly (colored as in panel a) in the transition from the holo-SOD1 to the reduced apo-SOD1 are shown in the surface representation.

dynamics resulting from misfolding. We compared the stability patch landscape of the intact holo-SOD1 with that of apo-SOD1, which represents a misfolded and potentially toxic SOD1 conformation.[16,17,20,35] The analysis has led us to the conclusion that the increased backbone mobility transforms certain surface regions of the misfolded SOD1 into structural equivalents of the interaction hot spots and has guided the identification of SOD1-derived peptides that bind SOD1 and alter the course of the amyloid aggregation of fALS SOD1 mutants.

RESULTS AND DISCUSSION

Misfolding Alters the Dynamics of SOD1 Surface Backbone. Demetalation and the reduction of the stabilizing intrasubunit disulfide bond are hallmarks of the conversion of the native SOD1 dimer into a noxious species.[16,17,20,35] We used SMD analysis to compare the dynamic properties of the surface backbone of the *monomers* of human WT holo-SOD1 and of the reduced, demetalated apo-SOD1 (C6A/C111A/C57A/C146A, which lacks any disulfide bond-forming potential).[20,36] Assuming that apo-SOD1 species represent the misfolded form of SOD1 with anomalous activities,[20,21] we expected this analysis to provide new insights into the molecular basis of the toxic gain-of-function of misfolded SOD1.

We found that the holo-SOD1 surface backbone is exceptionally rigid, because 53% of its surface-exposed residues are static. These static residues constituted a number of extended stability patches, the largest of which, as expected, is situated on the dimer interface (Figure 1a). In the apo-SOD1, by contrast, the overall content of static residues was significantly lower (42%), although several residues that were mobile in holo-SOD1 became static in the apo-SOD1 (Figure 2a,b). Consequently, the original stability patch landscape of holo-SOD1 was reshaped in apo-SOD1, such that a substantial portion of the surface backbone became mobile, with only 64% of the residues that were static in holo-SOD1 retaining their static character in apo-SOD1 (Figure 1b). This finding indicates that demetalation and disulfide bond reduction perturb the internal network of SOD1 structural constraints, some of which are relieved while others are reinforced. This change results in the formation of new misplaced stability patches and in the introduction of significant flexibility into the surface backbone.

Mechanism of the Acquired PPI Potential of Misfolded SOD1. Based on these observations and on our previous work,[31,32,34] we propose a mechanism for the gain-of-interaction of the misfolded SOD1. We suggest that the high stability patch content of the surface of the native SOD1 (holo-SOD1) endows it with a robust PPI potential but that this potential is almost completely "concealed" by the lack of

DOI: 10.1021/acschemneuro.6b00227
ACS Chem. Neurosci. 2016, 7, 1595−1606

backbone mobility, which is essential for structural adaptation and for the conversion of transient complexes into stable ones. In fact, the mechanical rigidity of protein surfaces, such as that characterized here for holo-SOD1, may serve to prevent nonspecific PPIs.[34] The formation of stable complexes between proteins with rigid surfaces requires a high degree of shape complementarity at the interface; in the absence of such complementarity, the enthalpic gain from the contacts at the interface is expected to weaken by the internal strains developed in the protein structure upon binding.[37] Thus, the exceptionally high rigidity of the surface of the native SOD1 may contribute to its appropriate functioning by preventing the aggregation of this highly abundant protein in the extremely crowded environment of biological solutions.

In its misfolded state (apo-SOD1), some of the internal constraints that rigidify the native SOD1 structure are released and surface areas of high backbone mobility emerge nearby the existing stability patches. In this scenario, surface adaptation at the interface (induced fit) becomes possible, thus converting distinct surface areas into structural analogs of the interaction "hot spots",[32,34] liberating the concealed PPI potential. As a result, the misfolded SOD1 may become "sticky" to acquire the ability to form oligomers and higher-order assemblies, which ultimately aggregate as amyloids. Moreover, when in solution, the misfolded SOD1 may form abnormal complexes with various other proteins. This structural transformation is probably not unique to SOD1, but since SOD1 is a highly abundant component of motor neurons,[33,38] its misfolded soluble species may present a significant threat to cell homeostasis by interacting with proteins that are crucial for cell functioning.[39] The selective damage to the motor neurons in ALS may also be explained by assuming that the motor neurons are absent of a specific molecular agent(s), whose activity is to protect cells from the misfolded SOD1 cytotoxicity.[40,41] The proposed "hot spot on the loose" gain-of-function mechanism may also hold true for other proteopathies, in which a misfolded protein is engaged in aberrant homologous (leading to aggregation) or heterologous PPIs.[42]

Notably, the extreme rigidity of the surface backbone may indicate an internally strained character of the holo-SOD1 structure. A metastable network of intramolecular interactions may be accountable for this phenomenon.[43] Because of its metastable character, the interaction network may collapse (at least partially) when some of the underlying interactions are obliterated by a mutation, metal loss, or disulfide reduction. In this case, the conformation of the holo-SOD1 may decay (relax) into a thermodynamically more stable "misfolded" state. The thermodynamic instability of the holo-SOD1 structure may explain the existence of an extraordinarily large number of point mutations, distributed throughout the entire SOD1 sequence, that cause SOD1 misfolding and amyloid formation leading to ALS.[7]

Stability Patch-Derived Peptides Bind SOD1. Under the assumption that the apo-SOD1 surface areas comprising the stability patch residues may form interfaces in aberrant protein complexes, we hypothesized that peptides derived from these regions may retain a residual capacity to bind target protein(s). Fourteen 20-mer peptides were derived from the stability patch regions of the apo-SOD1 (Figure 3a and Supplementary Figure S2) and tested for the ability to bind SOD1 proteins. The rational for using SOD1 as target was the notion that the mechanisms responsible for aberrant homologous and heterologous interactions are similar.

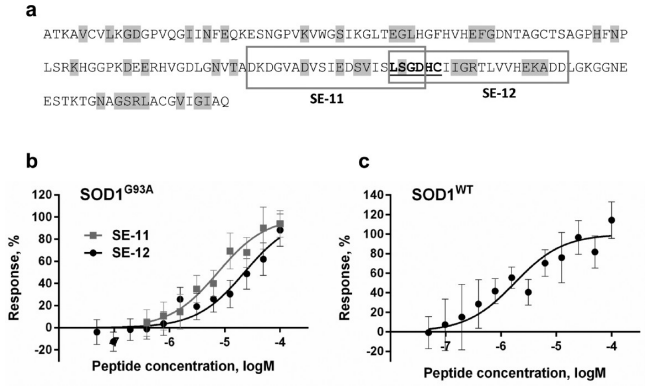

Figure 3. Peptides SE-11 and SE-12 interact with SOD1. (a) Distribution of "stability patch" residues (gray) along the SOD1 primary structure. The sequences of peptides SE-11 and SE-12 are indicated. The sequence that promoted peptide self-aggregation is shown in bold and underlined. Fluorescently labeled recombinant $SOD1^{G93A}$ (300 nM) (b) or $SOD1^{WT}$ (200 nM) (c) were incubated for 90 min at room temperature with increasing concentrations of SE-11 or SE-12, and the fluorescence was measured with an MST instrument. The changes in $SOD1^{WT}$ fluorescence in the presence of SE-11 were not plotted due to a low signal-to-noise ratio. The effects of both peptides on SOD1 fluorescence were abolished by protein denaturation (SD-denaturation test), indicating that a specific interaction with the peptide caused the observed changes in the SOD1 fluorescence. The curves represent the nonlinear regression analyses of the data using a three-parameter logistic function. The results are expressed as the mean ± SD of at least three independent experiments.

We expressed the $SOD1^{WT}$ and the $SOD1^{G93A}$ mutant[44] in *Escherichia coli* and purified them under nondenaturing conditions. An in-gel activity assay indicated that both proteins retained a residual enzymatic activity (Supplementary Figure S1a). The gel-filtration analysis demonstrated that $SOD1^{WT}$ and $SOD1^{G93A}$ were dimers and partially monomerized upon a prolonged incubation at 37 °C, during which $SOD1^{WT}$ remained fully soluble and $SOD1^{G93A}$ partially precipitated (Supplementary Figure S1b). Because *E. coli* is ineffective in promoting disulfide bond formation and metal incorporation into SOD1, the recombinant SOD1 proteins, without further treatment, appear to be a particularly appropriate model for studying the molecular mechanism of SOD1 pathology in ALS. The SOD1 proteins are most likely expressed in bacteria as a mixture of structural states at various stages of misfolding. Therefore, the recombinant SOD1 may closely mimic the endogenous human SOD1 under conditions of environmental stresses and reduced turnover, which are known to promote apo-SOD1 formation and misfolding.

The ability of the peptides to bind fluorescently labeled $SOD1^{WT}$ or $SOD1^{G93A}$ was tested by using the microscale thermophoresis (MST) technique.[45] We found two overlapping peptides, designated SE-11 (^{90}DKDGVADVSIEDSVIS-LSGD^{109}) and SE-12 (^{106}LSGDHCIIGRTLVVHEKADD^{125}), that caused a specific and dose-dependent increase in the fluorescence of the target SOD1 proteins. Specifically, SE-12 increased the fluorescence of both $SOD1^{WT}$ and $SOD1^{G93A}$, whereas SE-11 increased only the fluorescence of $SOD1^{G93A}$ (Figure 3a–c). The responses obtained with other peptides

DOI: 10.1021/acschemneuro.6b00227
ACS Chem. Neurosci. 2016, 7, 1595–1606

showed a low signal-to-noise ratio and, therefore, were not plotted.

In cells, the coexpression of $SOD1^{WT}$ and a fALS SOD1 mutant has been shown to aggravate ALS pathology, possibly due to the interaction between the two proteins and the prolongation of the solution lifetime of noxious species.[46,47] Moreover, the misfolded SOD1 has been proposed to be capable of propagating, in a prion-like manner, a toxic misfolding signal among structurally intact SOD1 proteins.[48,49]

Thus, although SOD^{WT} produced in *E. coli* may differ structurally or functionally from the holo-$SOD1^{WT}$ produced in eukaryotes, our finding that both $SOD1^{MUT}$ and $SOD1^{WT}$ can interact with the apo-SOD1-derived peptide is in agreement with these observations.

Stability Patch-Derived Peptides Affect the Kinetics of SOD1 Amyloid Aggregation and the Morphology of Aggregates. We predicted that the binding of the misfolded SOD1 to the peptides derived from its stability patch regions (SE-11 and SE-12) will affect its aggregation behavior. To test this prediction, we incubated $SOD1^{G93A}$ under aggregation-promoting conditions (i.e., in the presence of a reducing agent and a metal chelator) with increasing concentrations of SE-11 or SE-12 and measured the kinetics of amyloid aggregation by monitoring the fluorescence of thioflavin T (ThT) – a probe used to specifically detect amyloid aggregates.[9,50] In the absence of SE-11 or SE-12, $SOD1^{G93A}$ triggered a ThT response over the course of incubation, and TEM imaging at the end of the incubation period revealed the formation of fibrils (10–15 nm in width) and of small spherulites (0.1–0.2 μm in diameter) (Figure 4a,b and Figure 5a).

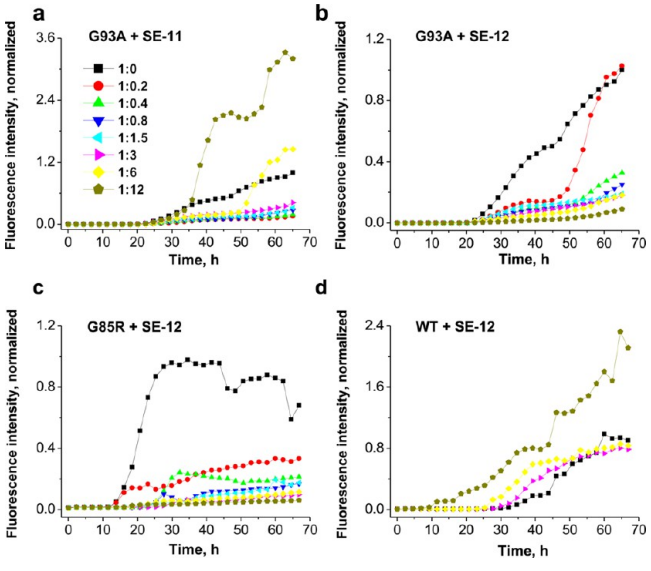

Figure 4. Peptides SE-11 and SE-12 affect the kinetics of amyloid aggregation of SOD1. ThT fluorescence was monitored in the course of $SOD1^{G93A}$ (50 μM) co-incubation with SE-11 (a) or SE-12 (b) at different molar ratios at 37 °C with continuous shaking. ThT fluorescence was monitored in the course of $SOD1^{G85R}$ (50 μM) (c) or $SOD1^{WT}$ (50 μM) (d) co-incubation with SE-12 at different molar ratios at 37 °C with continuous shaking. Values are normalized to the maximal ThT intensity elicited by $SOD1^{G93A}$, $SOD1^{G85R}$, or $SOD1^{WT}$ alone. All results are expressed as an average of assays performed in a triplicate in a representative experiment. Standard deviations of the kinetic traces were within 20% of the signal and were not depicted due to data normalization.

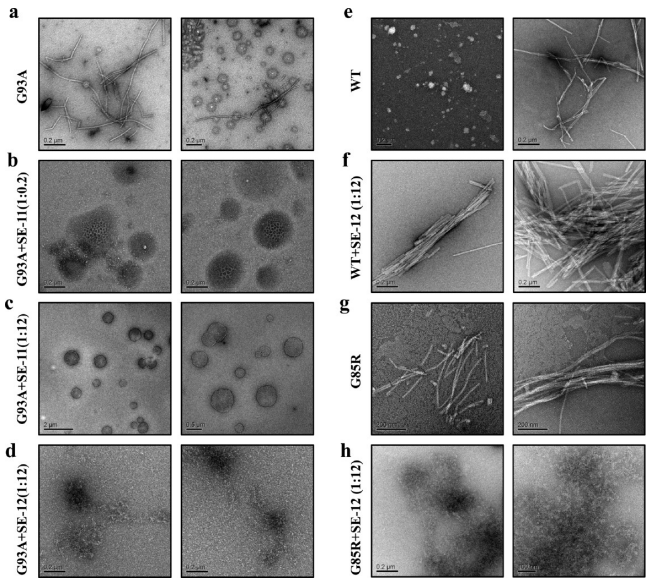

Figure 5. Peptides SE-11 and SE-12 affect the morphology of SOD1 aggregates. (a–d) TEM images of a $SOD1^{G93A}$ solution (50 μM) after an incubation of 65 h at 37 °C with continuous shaking. $SOD1^{G93A}$ was incubated either alone (a), in the presence of SE-11 at a molar ratio of 1:0.2 ($SOD1^{G93A}$/SE-11) (b), in the presence of SE-11 at a molar ratio of 1:12 (c), or in the presence of SE-12 at a molar ratio of 1:12 (d). (e,f) TEM images of a $SOD1^{WT}$ solution (50 μM) after 65 h of incubation at 37 °C with continuous shaking, in the absence (e) or presence (f) of SE-12 at a 1:12 molar ratio. (g,h) TEM images of a $SOD1^{G85R}$ solution (50 μM) after 65 h of incubation at 37 °C with continuous shaking, in the absence (g) or presence (h) of SE-12 at a 1:12 molar ratio.

At low peptide/SOD1 molar ratios, SE-11 inhibited the ThT response of $SOD1^{G93A}$ and suppressed the formation of the characteristic fibril-like aggregates; however, some amorphous aggregates and spherulites of irregular shapes and of various sizes were detected in the TEM analysis (Figure 4a and Figure 5b). In higher SE-11 concentrations (peptide/SOD1 molar ratio higher than 3), the inhibitory effect of SE-11 on the aggregation of $SOD1^{G93A}$ was reversed, such that the ThT response was significantly higher than that of $SOD1^{G93A}$ alone (Figure 4a and Figure 5c). In line with this finding, the TEM revealed that mainly large spherulites (0.5–1.0 μm in diameter) are formed at these molar ratios. When incubated alone at a concentration of 600 μM (the highest concentration tested here; see Figure 4a), the SE-11 peptide did not trigger any significant ThT response (Figure 6a), although the TEM revealed an abundance of minute (<5 nm in width) protofibril-like aggregates (Figure 6b(i)), which were not detected in the presence of $SOD1^{G93A}$ (Figure 5c).

In contrast with the SE-11 peptide, the SE-12 peptide inhibited the $SOD1^{G93A}$ ThT response in a dose-dependent manner (Figure 4b), and only amorphous aggregates were detected by TEM at the end of incubation (Figure 5d). Unlike SE-11, the SE-12 peptide demonstrated a strong self-aggregating behavior and formed large (15–20 nm in width) rod-shaped ThT-responsive fibrils (Figure 6a,b(ii)). The formation of self-aggregating SE-12 fibrils was completely abolished in the presence of $SOD1^{G93A}$, even at very low (e.g., 1:12) SOD1/peptide molar ratios (Figure 5d). Thus, the formation of amyloid ThT-responsive aggregates of $SOD1^{G93A}$ and SE-12 was mutually prevented when both were present in the solution.

DOI: 10.1021/acschemneuro.6b00227
ACS Chem. Neurosci. 2016, 7, 1595–1606

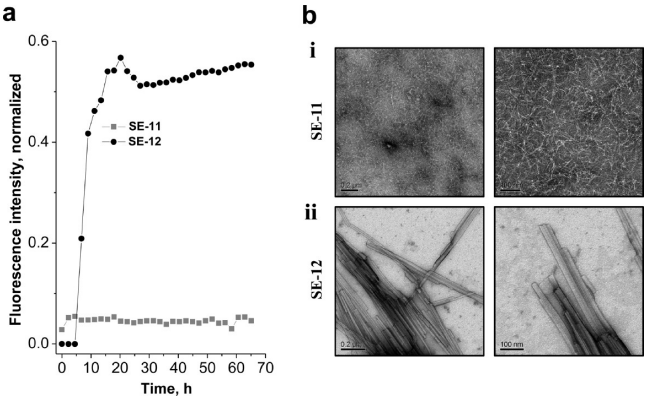

Figure 6. Self-aggregating properties of peptides SE-11 and SE-12. (a) ThT fluorescence was monitored in the course of SE-11 (600 μM) or SE-12 (600 μM) incubation at 37 °C with continuous shaking. The values were normalized to the maximal ThT intensity elicited by SOD1^{G93A} alone in the experiment shown in Figure 4a,b. All results are expressed as averages of assays performed in a triplicate in a representative experiment. (b) TEM images of peptides SE-11 (i) and SE-12 (ii) taken after incubation (65 h).

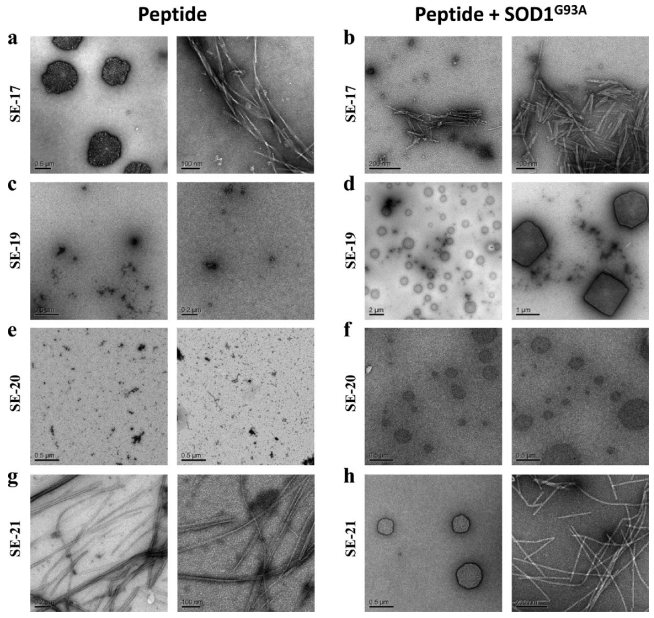

Figure 7. Peptides derived from the β6, β7, and β6/β7 loop region affect the morphology of SOD1^{G93A} aggregates. TEM images taken after incubation (65 h at 37 °C with continuous shaking) of SE-17, SE-19, SE-20, and SE-21, either alone (a, c, e, and g, respectively) or with SOD1^{G93A} (b, d, f, and h, respectively).

Taken together, the TEM studies indicated that the aggregation of misfolded SOD1 is not aborted in the presence of SE-12; rather, the peptide diverted the aggregation toward an alternative, amorphous pathway. To corroborate this notion, we used a turbidity assay to monitor the SOD1^{G93A} precipitation kinetics in the presence or absence of SE-12. This experiment revealed that, as was suggested by the TEM studies, SE-12 did not inhibit the aggregation of SOD1^{G93A} per se (Supplementary Figure S3).

To delineate the functional epitope of SE-11 and SE-12, we sampled sequences adjacent to the region of the SE-11/SE-12 overlap and tested the ability of the peptides to self-aggregate and affect the kinetics of amyloid aggregation of SOD1^{G93A} (Table 1). The presence of a short sequence, ^{106}LSGDHC^{111}, which corresponds to the SE-11/SE-12 overlap region, was sufficient to confer self-aggregating properties to the peptide and to facilitate the formation of ThT-responsive amyloid fibrils or spherulites. Peptides that lack this region (namely, SE-19 and SE-20) did not self-aggregate (Figure 7c,e, and data not shown), whereas SE-11, which contains an incomplete version of this sequence (^{106}LSGD^{109}), aggregated to form minute protofibril-like ThT-inert aggregates (see Figure 6, above). Co-incubating peptides SE-19 or SE-20 with SOD1^{G93A} resulted in the formation of ThT-responsive amyloid aggregates, whose morphology was different from that of the aggregates obtained with SOD1^{G93A} alone (Figure 7d,f, and data not shown).

In contrast to the self-aggregating SE-12, which inhibited the formation of amyloid SOD1^{G93A} aggregates, co-incubating the self-aggregating peptides SE-17 or SE-21 with SOD1^{G93A} did not prevent the formation of the ThT-responsive aggregates (Figure 7a,b,g,h, and data not shown). The morphology and size of these aggregates were different from those of the aggregates that were detected solely with SOD1^{G93A}. Since the molecular composition of the aggregates formed in the presence of SE-17 and SE-21 is unknown, it is unclear whether peptides SE-17 and SE-21 inhibit the amyloid aggregation of SOD1^{G93A}.

Because SE-12 was the only peptide in our study that inhibited the formation of amyloid aggregates in the presence of SOD1^{G93A}, we further characterized this peptide by evaluating its effect on the aggregation of SOD1^{WT} (with which, according to the binding assay, SE-12 can interact; see Figure 3b) and on the aggregation of another fALS mutant, SOD1^{G85R}.[51,52] A ThT assay under aggregation-promoting

Table 1. Analysis of Self-Aggregating Properties of Peptides Derived from β6, β7, and β6/β7 Loop Regions Reveals the Identity of the Aggregation-Initiating Sequence[a]

Name	Peptide sequence	ThT response	Structured aggregates (TEM)
SE-11	DKDGVADVSIEDSVIS**LSGD**	–	+
SE-12	**LSGDHC**IIGRTLVVHEKADD	++	++
SE-17	SIEDSVIS**LSGDHC**IIGRTLVVHEKADD	++	++
SE-19	IIGRTLVVHEKADD	–	–
SE-20	DKDGVADVSIEDSV	–	–
SE-21	EDSVIS**LSGDHC**IIGRT	++	++

[a]ThT fluorescence was monitored during an incubation of 65 h at 37 °C with continuous shaking. At the end of incubation, the samples were subjected to TEM imaging. The ^{106}LSGDHC^{111} region that exhibited aggregation-initiating properties is shown in bold and underlined.

DOI: 10.1021/acschemneuro.6b00227
ACS Chem. Neurosci. 2016, 7, 1595−1606

conditions demonstrated that the onset of SOD1 protein aggregation was the earliest for $SOD1^{G85R}$, followed by $SOD1^{G93A}$ and, finally, $SOD1^{WT}$ (Figure 4). This observation is consistent with the fact that the metal-deficient inactive $SOD1^{G85R}$ is more structurally destabilized than the wild-type-like $SOD1^{G93A}$ mutant.[51,52] At the end of the incubation period, $SOD1^{G85R}$ formed fibrillar aggregates (10−15 nm in width; Figure 5g), whereas $SOD1^{WT}$ demonstrated a variety of aggregation forms, including annular structures of irregular shape, fibrils, and minute amorphous aggregates (Figure 5e).

Similar to the aggregation-inhibiting effect of SE-12 on $SOD1^{G93A}$, SE-12 inhibited the amyloid aggregation of $SOD1^{G85R}$ in a dose-dependent manner, resulting in the formation of amorphous ThT-inert aggregates (Figure 4c and Figure 5h). Also similar to the experiments described above for $SOD1^{G93A}$ (Figure 5d), the self-aggregation of SE-12 to form rod-like ThT-responsive fibrils was completely abolished in the presence of $SOD1^{G85R}$ (Figure 5h). The similarity in the behavior of $SOD1^{G93A}$ and $SOD1^{G85R}$, two structurally and functionally dissimilar mutants,[52] in the presence of SE-12 suggests that the process of their structural transformation may follow a similar path and involve a common structural intermediate, which interacts with SE-12.

In contrast to the SOD1 mutants, the ThT response of $SOD1^{WT}$ to SE-12 was *enhanced* in a dose-dependent manner (Figure 4d), and TEM observations at the end of the incubation period indicated the formation of rod-like amyloid fibrils, which were similar to those formed by SE-12 alone (Figure 5f). Taken together with the increase in the ThT fluorescence, we believe that the formed fibrils belong to SE-12 and that the process of SE-12 *homologous* aggregation competes with the binding of SE-12 to SOD1. It is possible, for instance, that SE-12 interacts with the structural elements of $SOD1^{G93A}$ or $SOD1^{G85R}$, which are present in sufficient quantity and are kinetically accessible (i.e., surface-exposed) during the relatively short lag phase of SE-12 self-aggregation (Figure 6a), resulting in the abortion of the nucleation of the SE-12 self-aggregation. In contrast, the SE-12-interacting epitope on $SOD1^{WT}$ is kinetically inaccessible (or accessible to a lower degree), such that SE-12 self-aggregation prevails.

Proposed Mechanism of SOD1 Aggregation. The results above may prove instructive for understanding the process of amyloid aggregation by misfolded SOD1. In intact SOD1, the SE-12 aggregation-initiating sequence (^{106}LSGDHC^{111}) is part of the $\beta6/\beta7$ loop (the Greek Key loop). The $\beta6/\beta7$ loop is concealed within a surface cavity and its C-terminal part (^{111}CIIGR^{115}) is buried within the SOD1 dimer interface (Figure 8a). Under the assumption that the $\beta6/\beta7$ loop region is responsible for the initiation of amyloid aggregation, we hypothesized that the aggregation onset would require a subpopulation of SOD1 molecules to undergo misfolding, such that the hidden $\beta6/\beta7$ loop epitope is sufficiently exposed to mimic the action of the SE-12 peptide in solution (Scheme 1).

The exposure of the putative $\beta6/\beta7$ loop epitope can be achieved by an increased mobility of the surrounding substructures and, probably, separation of the SOD1 monomers. According to the SMD analysis, 63% (15/24) of the residues whose backbone mobility increased upon SOD1 misfolding (namely, residues S25, N26, P28, W32, T58, S59, P62, R69, P74, K75, E77, I99, H110, G108, and E121) are in close proximity to the SE-11 and SE-12 sequences, shaping the surface cavity that conceals the $\beta6/\beta7$ loop (Figure 8b). Thus,

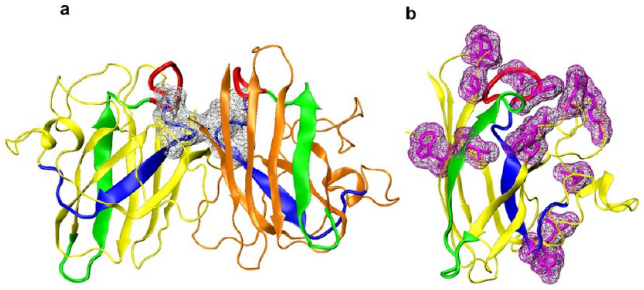

Figure 8. Exposure of the putative $\beta6/\beta7$ loop epitopes may require SOD1 misfolding. (a) The crystal structure of the apo-SOD1 dimer (PDB 2GBU) is shown in the cartoon representation, with individual monomers shown in orange and yellow. Sequences corresponding to the peptides are shown in green (SE-11) and blue (SE-12). The SE-11/SE-12 overlapping region identified as having aggregation-initiating properties (^{106}LSGDHC^{111}) is shown in red. The region of peptide SE-12 contributing to the formation of an intersubunit interface (^{111}CIIGR^{115}) is shown in the wireframe surface representation and is colored in gray. (b) One monomer of apo-SOD1. Sequences corresponding to the SE-11 and SE-12 peptides are colored as in panel a. The residues in the vicinity of SE-11 and SE-12 whose mobility increased upon SOD1 misfolding (Figure 2) are shown in the wireframe surface representation and are colored in magenta.

Scheme 1. Putative Mechanism of SOD1 Aggregation and Propagation of the Misfolding Signal[a]

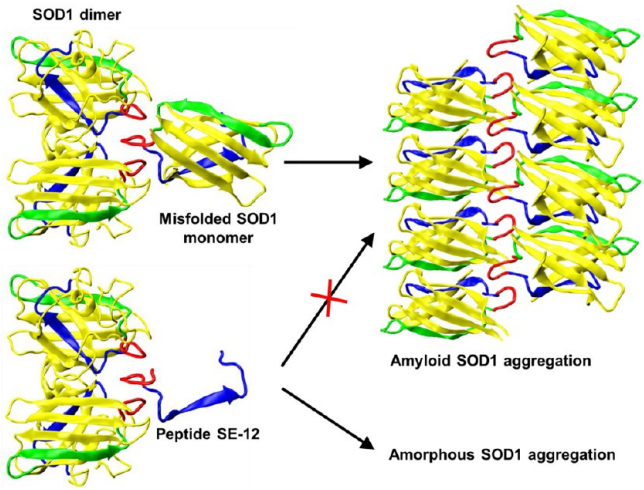

[a]Interaction of the putative aggregation-initiating sequence ^{106}LSGDHC^{111} in the $\beta6/\beta7$ loop (colored in red) of a misfolded SOD1 monomer induces the misfolding of a structurally intact SOD1 dimer. Monomers of the misfolded SOD1 may correspond to protomer units in amyloid aggregation. Aggregation is nucleated by interaction of the aggregation-initiating sequences in the $\beta6/\beta7$ loops from opposing protomers, followed by structural rearrangement and stabilization via auxiliary contacts mediated by the sequences corresponding to peptides SE-11 (in green) and SE-12 (in blue) on the opposite sides of the SOD1 β-barrel. The possible arrangement of SOD1 protomers within the structure of the amyloid fibrils is shown. Interaction of SOD1 with the isolated SE-12 peptide may interfere with the chain elongation process and result in the formation of scrambled (amorphous) aggregates of misfolded SOD1 molecules. The structure of the SOD1 β-barrel is colored in yellow.

in the apo-SOD1, the mobility of residues surrounding the putative $\beta6/\beta7$ loop epitope was increased, potentially contributing to its exposure. Notably, with S59, I99, and G108 as the only exceptions, none of the aforementioned

DOI: 10.1021/acschemneuro.6b00227
ACS Chem. Neurosci. 2016, 7, 1595−1606

residues is mutated in ALS,[5] suggesting that this region may bear functional importance for ALS pathogenesis.

On the other hand, in the intact SOD1 dimer, the $\beta6/\beta7$ loops of the two monomers are opposite to each other, and their planes are nearly parallel (Supplementary Figure S4). The space between the two $\beta6/\beta7$ loops is sufficiently large to accommodate an external polypeptide; thus, the monomeric SOD1, in which the putative $\beta6/\beta7$ loop epitope is exposed, may initiate amyloid aggregation by engaging the corresponding loop region in the target dimer, thereby destabilizing the dimer interface and facilitating the exposure of auxiliary epitopes required for oligomerization and fibril formation (Scheme 1). Such a mechanism may also rationalize the ability of the misfolding signal to propagate in a prion-like manner among structurally intact SOD1 proteins, thus spreading the disease in the nervous tissue.[48,49]

By using a computational algorithm, Khare et al. predicted that certain SOD1 regions, including the N- and C-termini, two crossover loops, and two β-strands in the Greek Key native fold, should have an increased propensity for oligomerization.[35] Similarly, Ivanova et al. used an alternative computational approach and identified SOD1 regions that are prone to fibril formation.[53] Based on its sequence and 3D conformation, the authors predicted that ^{101}DSVISLS^{107}, a region located within the Greek Key loop and within the SE-11 sequence, has a high propensity to form fibrils,[53] with residues ^{101}DSV^{103} contributing most of the Rosetta energy to form a putative steric zipper structure.[54] Whereas the study of Ivanova et al. indicated that the isolated peptide DSVISLS forms fibril-like ThT-inert aggregates,[53] this sequence did not promote self-aggregation of the peptides tested in our study (Table 1). A possible explanation for this discrepancy is that we used longer peptides than those used by Ivanova et al., such that the structural context of either the primary or the secondary structure adopted by the peptide in solution possibly affects the ability of internal sequence segments to promote aggregation. Similarly, in the context of the whole protein, SOD1 misfolding may alter the conformation of the $\beta6/\beta7$ loop, thus affecting the ability of internal segments to facilitate aggregation. However, an I104P substitution within the ^{101}DSVISLS^{107} sequence has been shown to suppress fibril formation by a full-length SOD1.[53] Residue I104 is adjacent to the ^{106}LSGDHC^{111} sequence, which we suggested to initiate amyloid aggregation, and the I104P substitution may have affected the conformation and backbone dynamics of the entire loop. Taken together, these findings are consistent with the idea that the $\beta6/\beta7$ loop region is involved in the initiation of amyloid aggregation by misfolded SOD1.

If the exposed $\beta6/\beta7$ loop epitope indeed acts as an initiator of the amyloid aggregation by misfolded SOD1, stabilizing the highly ordered structures of the emerging oligomers and amyloid protofibrils requires additional interactions. For instance, it is possible that the $\beta6$ and $\beta7$ strands, which are located at the opposite sides of the β-barrel of SOD1 and correspond to peptides SE-11 and SE-12, respectively, may contribute to this effect, for example, via β-sheet stacking contacts (Scheme 1). Peptides derived from the $\beta6$−loop−$\beta7$ region are expected to interfere with the ordered packing of SOD1 protomers. This interference will likely affect amyloid formation in a variety of ways, from chain termination and the formation of amorphous aggregates (as in the case of SE-12) to modifying the architecture (morphology) of the formed amyloids (as in the case of SE-11, and, possibly, of the other tested peptides).

According to the SMD analysis, several surface regions of the misfolded SOD1 possess the potential to form anomalous PPIs. Although the current study focused on aberrant interactions of the *homologous* type, which lead to amyloid aggregation, each of these putative surface epitopes may potentially mediate interactions with other proteins. To identify the epitopes involved in such a putative interaction between SOD1 and other proteins, the array of peptides described in this study (namely, the peptides that were derived from the stability patch regions of the apo-SOD1) should be screened for their ability to bind the protein in question.

The ability of the SE-12 peptide to redirect the aggregation of misfolded SOD1 from an amyloid aggregation pathway toward an amorphous disordered aggregation pathway may bear therapeutic consequences for ALS patients, because the surface epitopes responsible for the toxicity of misfolded SOD1 (namely, the epitopes responsible for its interaction with other proteins) may become scrambled or less accessible in amorphous aggregates. Indeed, amorphous aggregates are generally considered to be less toxic than amyloids, and their irregular microscopic structural organization usually results in a loss of function, rather than in a gain-of-function.[55−57]

METHODS

Preparation of Structures. For SMD analysis, we used equilibrated structures of SOD1 monomers extracted from the crystal structures of SOD1 dimers: PDB 1HL5 for the WT holo-SOD1 homodimer[36] and PDB 2GBU for the apo-SOD1 homodimer (C6A/C111A/C57A/C146A, lacking any disulfide bond forming potential).[20] To model the presence of coordinated metals in the structure of holo-SOD1, the distances among the Cu^{2+} [H46 (ND1), H48 (NE2), H63 (NE2), and H120 (NE2)] and Zn^{2+} [H63 (ND1), H71 (ND1), H80 (ND1), and D83 (OD1)] ligands were restrained in all simulations by applying extra bonded terms in the form of a harmonic energy potential $U(x) = k(x - x_{ref})^2$, with the spring constant k = 50.0 kcal/(mol·Å^2). The SOD1 monomer structures were solvated in a water box [50 × 54 × 54 Å^3 (13 044 atoms in total) for the holo-SOD1 and 57 × 49 × 54 Å^3 (13 639 atoms in total) for the apo-SOD1] using Na^+/Cl^- for charge neutralization, minimized, and equilibrated by using a molecular dynamics simulation with spatial constraints applied first to the whole protein (200 ps, water equilibration), then to the backbone atoms (100 ps), and finally without any spatial constraints, except for the distance constraints imitating the metal's presence in the holo-SOD1 (100 ps), time sufficient to equilibrate the system as revealed by the NAMD energy profile and RMSD variance of the protein atoms in trajectory. These and subsequent simulations were conducted in a isothermal−isobaric (NPT) ensemble at 310 K by using the NAMD program (version 2.9)[58] and the CHARMM27 force field for proteins.[59]

Steered Molecular Dynamics Simulation. A list of surface-exposed residues in the equilibrated structures of the SOD1 monomers was generated as described elsewhere.[34] The numbers of surface-exposed residues used in the SMD simulations were 95 and 97 for the holo-SOD1 and apo-SOD1, respectively. The SMD simulation was conducted for each surface residue without energy minimization by using the Cα atom as the SMD atom, as described elsewhere.[31,32] Briefly, the dummy atom was pulled at a *constant* velocity (0.15 Å/ps) in the direction of the vector connecting the Cα atom with the Cβ atom of a surface residue (in most cases, a direction approximating a normal to the local surface). During the simulation, no spatial constraints were applied to atoms within 15 Å of the SMD atom, whereas the Cα atoms outside the resulting 15 Å unconstrained hemisphere were set fixed. For each surface residue, the SMD simulation was repeated 12 times; applied forces were calculated from the SMD trajectories and plotted versus distances traveled by the dummy atoms. The plots were analyzed using a linear regression

DOI: 10.1021/acschemneuro.6b00227
ACS Chem. Neurosci. 2016, 7, 1595−1606

(Prism 6, GraphPad Software, Inc.), and the calculated slopes were referred to as the resistance coefficients (RC).[31,32]

The RC is a composite semiquantitative parameter that reflects two structural features directly related to PPIs.[31,34] The first is the local flexibility (conformational entropy) of the backbone. The higher the mobility of the recognition elements in the unbound state, the more adverse ΔS° results from their immobilization upon the complex formation. This component of the RC would correlate with Cα RMSD of thermal fluctuations calculated using an equilibrium molecular dynamics (EMD). The second component is unique to SMD capable of sampling local structural perturbations inaccessible by EMD. This component reflects the extent of the mechanical rigidity of local structures. If the recognition elements located within a stability patch are engaged in interaction, a strong favorable contribution to ΔH° will result only if there is a good structural (shape) complementarity of the binding surfaces. Otherwise, internal strains will be developed in the system upon binding reducing the enthalpic gain of interaction.[37] In this respect, the interfacial stability patches may contribute to defining the geometry and specificity of the complex formed.

The SOD1 dimer interface was delineated using the KFC (Knowledge-based FADE and Contacts) server.[60] Structures were visualized and images were generated by using the VMD software.[61]

Purification and Evaluation of Recombinant SOD1^{WT}, SOD1^{G93A}, and SOD1^{G85R} proteins. Sequences of human SOD1^{WT}, SOD1^{G93A}, and SOD1^{G85R} were optimized for codon usage in *E. coli*, cloned into pHIS1 vector[62] and expressed as 6His-tagged (N-term) soluble proteins in BL21 cells. Cells were grown in LB medium containing 100 μg/mL ampicillin at 30 °C for 4 h and the expression of the recombinant SOD1 proteins was induced by addition of 0.1 mM IPTG, followed by overnight incubation at 20 °C. Cells were harvested by 25 min centrifugation (4000 × *g*) at 4 °C. After 30 min incubation on ice, the cells were disrupted by sonication in a loading buffer (50 mM Na^+/phosphate, pH 7.6, 0.5 M NaCl, 2 mM β-mercaptoethanol, 10 mM imidazole) containing 1 mg/mL lysozyme and a protease inhibitor cocktail (Sigma, Israel). To remove DNA, the crude extract was incubated on ice for 30 min in the presence of 100 U/mL bovine pancreas DNaseI (Sigma, Israel) and 5 mM $MgSO_4$, followed by 30 min centrifugation (20000 × *g*) at 4 °C. The supernatant was loaded on a 5-mL HisTrap FF column (GE Healthcare Life Sciences, Sweden) equilibrated with the loading buffer. The column was washed with five column volumes (CV) of a washing buffer (50 mM Na^+/phosphate, pH 7.6, 0.5 M NaCl, 2 mM β-mercaptoethanol, 20 mM imidazole), and the protein was eluted by a linear 20−400 mM imidazole gradient (10 CV). The peak fractions were dialyzed overnight at 4 °C against a storage buffer (50 mM Na^+/phosphate, pH 7.6, 0.1 M NaCl, and 10% glycerol), concentrated by ultrafiltration (10 kDa cutoff, Millipore, USA), centrifuged at 110000 × *g* at 4 °C for 1 h using ultracentrifuge (Sorvall M120, Discovery), and the supernatant stored at −20 °C until use. Protein concentration was measured by the Bradford method using bovine serum albumin as standard.

The enzymatic activities of SOD1^{WT} and SOD1^{G93A} were assessed by an in-gel activity assay as described elsewhere.[63] Protein samples (20 μg) were separated on a 10% native polyacrylamide gel. The gel was stained in a dark environment using a solution containing 0.3 mM riboflavin, 0.3 mM nitro blue tetrazolium (NBT), and 1% TEMED and kept under a white light for 30 min at rt.

For size exclusion chromatography, purified SOD1^{WT} and SOD1^{G93A} were incubated at 37 °C in 50 mM Na^+/phosphate buffer, pH 7.6, containing 0.1 M NaCl, 1 mM EDTA, and 1 mM TCEP for the indicated time and separated on Superdex 200 10/300 GL column (GE Healthcare Life Sciences, Sweden) at flow rate of 0.5 mL/min using 50 mM Na^+/phosphate, pH 7.6, 0.1 M NaCl as running buffer.

Peptide Binding to SOD1. Peptides were synthesized by GL Biochem Ltd. (Shanghai, China). Peptide identity and purity (>90%) was confirmed by MS and HPLC analyses. For microscale thermophoresis (MST) analysis,[45] the proteins (SOD1^{WT} and SOD1^{G93A}) were labeled with BLUE fluorescent dye NT-495-NHS (lysine chemistry) using a Monolith NT protein labeling kit Blue-NHS (Nano Temper Technologies, München, Germany) at a protein (monomer)/dye ratio of 1:3 as recommended by the manufacturer.

The assessment of peptide binding to the proteins was carried out using Monolith NT.115 (NanoTemper Technologies, München, Germany). The labeled SOD1^{WT} (200 nM) or SOD1^{G93A} (300 nM) was incubated for 1.5 h in 50 mM Na^+/phosphate binding buffer, pH 7.6, 0.1 M NaCl, 0.1 mM TCEP, 0.04% Tween-20, and 1 mg/mL BSA at rt with increasing concentrations of peptide (0−100 μM) dissolved in DMSO or DMF (if the peptide contained cysteine residues). The final concentration of either DMSO or DMF in the binding buffer was 1%. The SD-denaturation test, in which samples were incubated for 5 min at 95 °C in the presence of 4% SDS and 40 mM DTT, was performed according to the manufacturer's instructions. The binding data were analyzed by a nonlinear regression using a logistic (three parameter) function implemented in Prism6 (GraphPad) program.

ThT Aggregation Assay for SOD1 and SOD1-Derived Peptides. Prior to the aggregation assay, all mixtures containing protein or peptide were filtered through a 0.22 μm Millex-GV (PVDF) syringe filter, 4 mm (Millipore, USA). SOD1 (WT, G93A, or G85R; 50 μM) with or without a peptide was incubated in 200 μL of 20 mM Na^+/phosphate buffer, pH 7.0, 0.1 M NaCl, 5 mM EDTA, 1 mM TCEP, and 1% DMF in the presence of 50 μM thioflavin T (Sigma-Aldrich, Israel) in a black 96-well plate at 37 °C with continuous shaking (set to fast) using a SpectraMax Paradigm (Molecular Devices) ELISA reader. The fluorescence (exc 440 nm; em 485 nm) was measured at 10 min intervals.

Analysis of SOD1 Fibril Formation by Transmission Electron Microscopy (TEM). Samples for TEM imaging were prepared as described elsewhere.[64] Briefly, at the end of the aggregation assay, 2.5 μL samples (diluted 5-fold) were deposited on a carbon-coated copper 300 mesh. After 1 min, the excess liquid was carefully blotted by a filter paper. Following 1 min drying at ambient temperature, 5 μL of 2% uranyl acetate was added. After 1 min, the excess of the salt solution was carefully removed with a filter paper. The imaging was performed using a Tecnai G2 12 BioTWIN (FEI) transmission electron microscope with an acceleration voltage of 120 kV. Depending on the aggregate size, different magnifications were used. The visible features were sensitive to the electron beam exposure, indicating their organic origin.

Turbidity Aggregation Assay for SOD1. Aggregation kinetics of SOD^{G93A} (50 μM) in the presence or absence of the SE-12 peptide (300 μM) was measured spectroscopically at 405 nm in 20 mM Na^+/phosphate buffer, pH 7.6, 1 mM TCEP, 5 mM EDTA, and 0.1 M NaCl. The mixture was incubated at 37 °C for 15 h, after which the shaking (1000 rpm) was applied. The turbidity was measured at the indicated time intervals using the Ultrospec 7000 spectrophotometer (GE Healthcare).

■ ASSOCIATED CONTENT

Supporting Information

The Supporting Information is available free of charge on the ACS Publications website at DOI: 10.1021/acschemneuro.6b00227.

Description of the structural and function evaluation of the SOD1 recombinant proteins (Figure S1), design of SOD1-derived peptides (Figure S2), SOD1 aggregation analysis (Figure S3), and the structure of the SOD1 dimer demonstrating the surface cavity formed by the two β6/β7 loops (Figure S4) (PDF)

■ AUTHOR INFORMATION

Corresponding Author

*Dr. Stanislav Engel. Mailing address: Department of Clinical Biochemistry and Pharmacology, Faculty of Health Sciences, Ben-Gurion University of the Negev, P.O.B. 653, Beer-Sheva 8410501, Israel. Phone: +972-86428593. Fax: +972-86479012. E-mail: engels@bgu.ac.il.

DOI: 10.1021/acschemneuro.6b00227
ACS Chem. Neurosci. 2016, 7, 1595−1606

Author Contributions

Conceptualization, S.E.; methodology, S.E., A.I., N.P., V.B. and T.S.; investigation, V.B., T.S., B.K. and M.V.; writing, original draft, S.E.; writing, review and editing, S.E., A.I., N.P., V.B., and T.S.; resources, S.E., A.I., and N.P.; supervision, S.E., A.I., and N.P.

Funding

This work was supported in part by the internal grant from the National Institute for Biotechnology in the Negev, Israel, and 124/14 grant from the Israel Science Foundation. N.P. acknowledges the support from the European Research Council "Ideas program" ERC-2013-StG (Contract Grant Number 336041).

Notes

The authors declare no competing financial interest.

■ ACKNOWLEDGMENTS

We thank Olga Press, Tatiana Zvagelsky, Guy Zoltsman, and Dr. Salah Abu-Hamad for their help in the preparation of this manuscript. We also thank Dr. Zeev Barak for critical reading of the manuscript.

■ ABBREVIATIONS

ALS, amyotrophic lateral sclerosis; PPIs, protein−protein interactions; SMD, steered molecular dynamics; SOD1, superoxide dismutase 1

■ REFERENCES

(1) Carrell, R. W., and Lomas, D. A. (1997) Conformational disease. *Lancet 350*, 134−138.

(2) Selkoe, D. J. (2003) Folding proteins in fatal ways. *Nature 426*, 900−904.

(3) Miller, R. G., Mitchell, J. D., Lyon, M., and Moore, D. H. (2003) Riluzole for amyotrophic lateral sclerosis (ALS)/motor neuron disease (MND). *Amyotrophic Lateral Scler. Other Mot. Neuron Disord. 4*, 191−206.

(4) Han-Xiang, D., Hujun, J., Ronggen, F., Hong, Z., Yong, S., Erdong, L., Makito, H., Mauro, C. D. C., and Teepu, S. (2008) Molecular dissection of ALS-associated toxicity of SOD1 in transgenic mice using an exon-fusion approach. *Hum. Mol. Genet. 17*, 2310−2319.

(5) Abel, O., Powell, J. F., Andersen, P. M., and Al-Chalabi, A. (2012) ALSoD: A user-friendly online bioinformatics tool for amyotrophic lateral sclerosis genetics. *Hum. Mutat. 33*, 1345−1351.

(6) Rosen, D. R., Siddique, T., Patterson, D., Figlewicz, D. A., Sapp, P., Hentati, A., Donaldson, D., Goto, J., O'Regan, J. P., Deng, H.-X., Rahmani, Z., Krizus, A., McKenna-Yasek, D., Cayabyab, A., Gaston, S. M., Berger, R., Tanzi, R. E., Halperin, J. J., Herzfeldt, B., Van den Bergh, R., Hung, W.-Y., Bird, T., Deng, G., Mulder, D. W., Smyth, C., Laing, N. G., Soriano, E., Pericak-Vance, M. A., Haines, J., Rouleau, G. A., Gusella, J. S., Horvitz, H. R., and Brown, R. H. (1993) Mutations in Cu/Zn superoxide dismutase gene are associated with familial amyotrophic lateral sclerosis. *Nature 362*, 59−62.

(7) Battistini, S., Giannini, F., Greco, G., Bibbò, G., Ferrera, L., Marini, V., Causarano, R., Casula, M., Lando, G., Patrosso, M. C., Caponnetto, C., Origone, P., Marocchi, A., Del Corona, A., Siciliano, G., Carrera, P., Mascia, V., Giagheddu, M., Carcassi, C., Orrù, S., Garrè, C., and Penco, S. (2005) SOD1 mutations in amyotrophic lateral sclerosis. *J. Neurol. 252*, 782−788.

(8) Al-Chalabi, A., and Leigh, P. N. (2000) Recent advances in amyotrophic lateral sclerosis. *Curr. Opin. Neurol. 13*, 397−405.

(9) Leal, S. S., Cardoso, I., Valentine, J. S., and Gomes, C. M. (2013) Calcium Ions Promote Superoxide Dismutase 1 (SOD1) Aggregation into Non-fibrillar Amyloid: A Link to Toxic Effects of Calcium Overload in Amyotrophic Lateral Sclerosis (ALS)? *J. Biol. Chem. 288*, 25219−25228.

(10) Forsberg, K., Jonsson, P. A., Andersen, P. M., Bergemalm, D., Graffmo, K. S., Hultdin, M., Jacobsson, J., Rosquist, R., Marklund, S. L., and Brännström, T. (2010) Novel Antibodies Reveal Inclusions Containing Non-Native SOD1 in Sporadic ALS Patients. *PLoS One 5*, e11552.

(11) Bruijn, L. I., Miller, T. M., and Cleveland, D. W. (2004) Unraveling the Mechanisms Involved in Motor Neuron Degeneration in ALS. *Annu. Rev. Neurosci. 27*, 723−749.

(12) Gurney, M. E., Pu, H., Chiu, A. Y., Dal Canto, M. C., Polchow, C. Y., Alexander, D. D., Caliendo, J., Hentati, A., Kwon, Y. W., Deng, H. X., et al. (1994) Motor neuron degeneration in mice that express a human Cu,Zn superoxide dismutase mutation. *Science 264*, 1772−1775.

(13) Bruijn, L. I., Houseweart, M. K., Kato, S., Anderson, K. L., Anderson, S. D., Ohama, E., Reaume, A. G., Scott, R. W., and Cleveland, D. W. (1998) Aggregation and motor neuron toxicity of an ALS-linked SOD1 mutant independent from wild-type SOD1. *Science 281*, 1851−1854.

(14) Wong, P. C., Pardo, C. A., Borchelt, D. R., Lee, M. K., Copeland, N. G., Jenkins, N. A., Sisodia, S. S., Cleveland, D. W., and Price, D. L. (1995) An adverse property of a familial ALS-linked SOD1 mutation causes motor neuron disease characterized by vacuolar degeneration of mitochondria. *Neuron 14*, 1105−1116.

(15) Zhao, W., Beers, D. R., Henkel, J. S., Zhang, W., Urushitani, M., Julien, J.-P., and Appel, S. H. (2010) Extracellular Mutant SOD1 Induces Microglial-Mediated Motoneuron Injury. *Glia 58*, 231−243.

(16) Banci, L., Bertini, I., Durazo, A., Girotto, S., Gralla, E. B., Martinelli, M., Valentine, J. S., Vieru, M., and Whitelegge, J. P. (2007) Metal-free superoxide dismutase forms soluble oligomers under physiological conditions: A possible general mechanism for familial ALS. *Proc. Natl. Acad. Sci. U. S. A. 104*, 11263−11267.

(17) Oztug Durer, Z. A., Cohlberg, J. A., Dinh, P., Padua, S., Ehrenclou, K., Downes, S., Tan, J. K., Nakano, Y., Bowman, C. J., Hoskins, J. L., Kwon, C., Mason, A. Z., Rodriguez, J. A., Doucette, P. A., Shaw, B. F., and Valentine, J. S. (2009) Loss of Metal Ions, Disulfide Reduction and Mutations Related to Familial ALS Promote Formation of Amyloid-Like Aggregates from Superoxide Dismutase. *PLoS One 4*, e5004.

(18) Ray, S. S., Nowak, R. J., Strokovich, K., Brown, R. H., Jr., Walz, T., and Lansbury, P. T., Jr. (2004) An Intersubunit Disulfide Bond Prevents in Vitro Aggregation of a Superoxide Dismutase-1 Mutant Linked to Familial Amytrophic Lateral Sclerosis. *Biochemistry 43*, 4899−4905.

(19) Brown, N. M., Torres, A. S., Doan, P. E., and O'Halloran, T. V. (2004) Oxygen and the copper chaperone CCS regulate posttranslational activation of Cu,Zn superoxide dismutase. *Proc. Natl. Acad. Sci. U. S. A. 101*, 5518−5523.

(20) Hörnberg, A., Logan, D. T., Marklund, S. L., and Oliveberg, M. (2007) The Coupling between Disulphide Status, Metallation and Dimer Interface Strength in Cu/Zn Superoxide Dismutase. *J. Mol. Biol. 365*, 333−342.

(21) Liu, H.-N., Tjostheim, S., DaSilva, K., Taylor, D., Zhao, B., Rakhit, R., Brown, M., Chakrabartty, A., McLaurin, J., and Robertson, J. (2012) Targeting of Monomer/Misfolded SOD1 as a Therapeutic Strategy for Amyotrophic Lateral Sclerosis. *J. Neurosci. 32*, 8791−8799.

(22) Zhai, J., Lin, H., Canete-Soler, R., and Schlaepfer, W. W. (2005) HoxB2 binds mutant SOD1 and is altered in transgenic model of ALS. *Hum. Mol. Genet. 14*, 2629−2640.

(23) Mali, Y., and Zisapels, N. (2008) Gain of interaction of ALS-linked G93A superoxide dismutase with cytosolic malate dehydrogenase. *Neurobiol. Dis. 32*, 133−141.

(24) Mali, Y., and Zisapel, N. (2009) A Novel Decoy That Interrupts G93A-Superoxide Dismutase Gain of Interaction with Malate Dehydrogenase Improves Survival in an Amyotrophic Lateral Sclerosis Cell Model. *J. Med. Chem. 52*, 5442−5448.

(25) Israelson, A., Arbel, N., Da Cruz, S., Ilieva, H., Yamanaka, K., Shoshan-Barmatz, V., and Cleveland, D. W. (2010) Misfolded Mutant SOD1 Directly Inhibits VDAC1 Conductance in a Mouse Model of Inherited ALS. *Neuron 67*, 575−587.

DOI: 10.1021/acschemneuro.6b00227
ACS Chem. Neurosci. 2016, 7, 1595−1606

(26) Pedrini, S., Sau, D., Guareschi, S., Bogush, M., Brown, R. H., Naniche, N., Kia, A., Trotti, D., and Pasinelli, P. (2010) ALS-linked mutant SOD1 damages mitochondria by promoting conformational changes in Bcl-2. *Hum. Mol. Genet. 19*, 2974−2986.
(27) Agbas, A., Hui, D., Wang, X., Tek, V., Zaidi, A., and Michaelis, E. K. (2007) Activation of brain calcineurin (Cn) by Cu-Zn superoxide dismutase (SOD1) depends on direct SOD1−Cn protein interactions occurring in vitro and in vivo. *Biochem. J. 405*, 51−59.
(28) Zhang, F., Ström, A.-L., Fukada, K., Lee, S., Hayward, L. J., and Zhu, H. (2007) Interaction between Familial Amyotrophic Lateral Sclerosis (ALS)-linked SOD1Mutants and the Dynein Complex. *J. Biol. Chem. 282*, 16691−16699.
(29) Nishitoh, H., Kadowaki, H., Nagai, A., Maruyama, T., Yokota, T., Fukutomi, H., Noguchi, T., Matsuzawa, A., Takeda, K., and Ichijo, H. (2008) ALS-linked mutant SOD1 induces ER stress- and ASK1-dependent motor neuron death by targeting Derlin-1. *Genes Dev. 22*, 1451−1464.
(30) Zetterström, P., Graffmo, K. S., Andersen, P. M., Brännström, T., and Marklund, S. L. (2011) Proteins That Bind to Misfolded Mutant Superoxide Dismutase-1 in Spinal Cords from Transgenic Amyotrophic Lateral Sclerosis (ALS) Model Mice. *J. Biol. Chem. 286*, 20130−20136.
(31) Kuttner, Y. Y., Nagar, T., and Engel, S. (2013) Surface Dynamics in Allosteric Regulation of Protein-Protein Interactions: Modulation of Calmodulin Functions by Ca^{2+}. *PLoS Comput. Biol. 9*, e1003028.
(32) Kuttner, Y. Y., and Engel, S. (2012) Protein hot spots: the islands of stability. *J. Mol. Biol. 415*, 419−428.
(33) Pardo, C. A., Xu, Z., Borchelt, D. R., Price, D. L., Sisodia, S. S., and Cleveland, D. W. (1995) Superoxide dismutase is an abundant component in cell bodies, dendrites, and axons of motor neurons and in a subset of other neurons. *Proc. Natl. Acad. Sci. U. S. A. 92*, 954−958.
(34) Osman, R., Mezei, M., and Engel, S. (2016) The role of protein "Stability patches" in molecular recognition: A case study of the human growth hormone-receptor complex. *J. Comput. Chem. 37*, 913−919.
(35) Khare, S. D., Wilcox, K. C., Gong, P., and Dokholyan, N. V. (2005) Sequence and structural determinants of Cu, Zn superoxide dismutase aggregation. *Proteins: Struct., Funct., Genet. 61*, 617−632.
(36) Strange, R. W., Antonyuk, S., Hough, M. A., Doucette, P. A., Rodriguez, J. A., Hart, P. J., Hayward, L. J., Valentine, J. S., and Hasnain, S. S. (2003) The Structure of Holo and Metal-deficient Wild-type Human Cu, Zn Superoxide Dismutase and its Relevance to Familial Amyotrophic Lateral Sclerosis. *J. Mol. Biol. 328*, 877−891.
(37) Jen-Jacobson, L., Engler, L. E., and Jacobson, L. A. (2000) Structural and Thermodynamic Strategies for Site-Specific DNA Binding Proteins. *Structure 8*, 1015−1023.
(38) Sun, S. Y., Sun, Y., Ling, S. C., Ferraiuolo, L., McAlonis-Downes, M., Zou, Y. Y., Drenner, K., Wang, Y., Ditsworth, D., Tokunaga, S., Kopelevich, A., Kaspar, B. K., Lagier-Tourenne, C., and Cleveland, D. W. (2015) Translational profiling identifies a cascade of damage initiated in motor neurons and spreading to glia in mutant SOD1-mediated ALS. *Proc. Natl. Acad. Sci. U. S. A. 112*, E6993−E7002.
(39) Proctor, E. A., Fee, L., Tao, Y., Redler, R. L., Fay, J. M., Zhang, Y., Lv, Z., Mercer, I. P., Deshmukh, M., Lyubchenko, Y. L., and Dokholyan, N. V. (2016) Nonnative SOD1 trimer is toxic to motor neurons in a model of amyotrophic lateral sclerosis. *Proc. Natl. Acad. Sci. U. S. A. 113*, 614.
(40) Israelson, A., Ditsworth, D., Sun, S., Song, S., Liang, J., Hruska-Plochan, M., McAlonis-Downes, M., Abu-Hamad, S., Zoltsman, G., Shani, T., Maldonado, M., Bui, A., Navarro, M., Zhou, H., Marsala, M., Kaspar, B. K., Da Cruz, S., and Cleveland, D. W. (2015) Macrophage migration inhibitory factor as a chaperone inhibiting accumulation of misfolded SOD1. *Neuron 86*, 218−232.
(41) Leyton-Jaimes, M. F., Benaim, C., Abu-Hamad, S., Kahn, J., Guetta, A., Bucala, R., and Israelson, A. (2016) Endogenous Macrophage Migration Inhibitory Factor Reduces the Accumulation and Toxicity of Misfolded SOD1 in a Mouse Model of ALS. *Proc. Natl. Acad. Sci. U. S. A.*, DOI: 10.1073/pnas.1604600113.
(42) Bucciantini, M., Giannoni, E., Chiti, F., Baroni, F., Formigli, L., Zurdo, J., Taddei, N., Ramponi, G., Dobson, C. M., and Stefani, M. (2002) Inherent toxicity of aggregates implies a common mechanism for protein misfolding diseases. *Nature 416*, 507−511.
(43) Das, A., and Plotkin, S. S. (2013) SOD1 exhibits allosteric frustration to facilitate metal binding affinity. *Proc. Natl. Acad. Sci. U. S. A. 110*, 3871−3876.
(44) Valentine, J. S., and Hart, P. J. (2003) Misfolded CuZnSOD and amyotrophic lateral sclerosis. *Proc. Natl. Acad. Sci. U. S. A. 100*, 3617−3622.
(45) Wienken, C. J., Baaske, P., Rothbauer, U., Braun, D., and Duhr, S. (2010) Protein-binding assays in biological liquids using microscale thermophoresis. *Nat. Commun. 1*, 100.
(46) Prudencio, M., Durazo, A., Whitelegge, J. P., and Borchelt, D. R. (2010) An examination of wild-type SOD1 in modulating the toxicity and aggregation of ALS-associated mutant SOD1. *Hum. Mol. Genet. 19*, 4774−4789.
(47) Qualls, D., Prudencio, M., Roberts, B., Crosby, K., Brown, H., and Borchelt, D. (2013) Features of wild-type human SOD1 limit interactions with misfolded aggregates of mouse G86R Sod1. *Mol. Neurodegener. 8*, 46.
(48) Ayers, J., Fromholt, S., Koch, M., DeBosier, A., McMahon, B., Xu, G., and Borchelt, D. (2014) Experimental transmissibility of mutant SOD1 motor neuron disease. *Acta Neuropathol. 128*, 791.
(49) Munch, C., O'Brien, J., and Bertolotti, A. (2011) Prion-like propagation of mutant superoxide dismutase-1 misfolding in neuronal cells. *Proc. Natl. Acad. Sci. U. S. A. 108*, 3548−3553.
(50) Banerjee, V., Kar, R. K., Datta, A., Parthasarathi, K., Chatterjee, S., Das, K. P., and Bhunia, A. (2013) Use of a Small Peptide Fragment as an Inhibitor of Insulin Fibrillation Process: A Study by High and Low Resolution Spectroscopy. *PLoS One 8*, e72318.
(51) Cao, X., Antonyuk, S. V., Seetharaman, S. V., Whitson, L. J., Taylor, A. B., Holloway, S. P., Strange, R. W., Doucette, P. A., Valentine, J. S., Tiwari, A., Hayward, L. J., Padua, S., Cohlberg, J. A., Hasnain, S. S., and Hart, P. J. (2008) Structures of the G85R Variant of SOD1 in Familial Amyotrophic Lateral Sclerosis. *J. Biol. Chem. 283*, 16169−16177.
(52) Hayward, L. J., Rodriguez, J. A., Kim, J. W., Tiwari, A., Goto, J. J., Cabelli, D. E., Valentine, J. S., and Brown, R. H., Jr. (2002) Decreased metallation and activity in subsets of mutant superoxide dismutases associated with familial amyotrophic lateral sclerosis. *J. Biol. Chem. 277*, 15923−15931.
(53) Ivanova, M. I., Sievers, S. A., Guenther, E. L., Johnson, L. M., Winkler, D. D., Galaleldeen, A., Sawaya, M. R., Hart, P. J., and Eisenberg, D. S. (2014) Aggregation-triggering segments of SOD1 fibril formation support a common pathway for familial and sporadic ALS. *Proc. Natl. Acad. Sci. U. S. A. 111*, 197−201.
(54) Goldschmidt, L., Teng, P. K., Riek, R., and Eisenberg, D. (2010) Identifying the amylome, proteins capable of forming amyloid-like fibrils. *Proc. Natl. Acad. Sci. U. S. A. 107*, 3487−3492.
(55) Bednarska, N. G., Schymkowitz, J., Rousseau, F., and Van Eldere, J. (2013) Protein aggregation in bacteria: the thin boundary between functionality and toxicity. *Microbiology 159*, 1795−1806.
(56) Stefani, M., and Rigacci, S. (2013) Protein Folding and Aggregation into Amyloid: The Interference by Natural Phenolic Compounds. *Int. J. Mol. Sci. 14*, 12411−12457.
(57) Bhatia, N. K., Srivastava, A., Katyal, N., Jain, N., Khan, M. A., Kundu, B., and Deep, S. (2015) Curcumin binds to the pre-fibrillar aggregates of Cu/Zn superoxide dismutase (SOD1) and alters its amyloidogenic pathway resulting in reduced cytotoxicity. *Biochim. Biophys. Acta, Proteins Proteomics 1854*, 426−436.
(58) Phillips, J. C., Braun, R., Wang, W., Gumbart, J., Tajkhorshid, E., Villa, E., Chipot, C., Skeel, R. D., Kalé, L., and Schulten, K. (2005) Scalable molecular dynamics with NAMD. *J. Comput. Chem. 26*, 1781−1802.
(59) MacKerell, A. D., Bashford, D., Bellott, Dunbrack, R. L., Evanseck, J. D., Field, M. J., Fischer, S., Gao, J., Guo, H., Ha, S., Joseph-McCarthy, D., Kuchnir, L., Kuczera, K., Lau, F. T. K., Mattos, C., Michnick, S., Ngo, T., Nguyen, D. T., Prodhom, B., Reiher, W. E.,

DOI: 10.1021/acschemneuro.6b00227
ACS Chem. Neurosci. 2016, 7, 1595−1606

Roux, B., Schlenkrich, M., Smith, J. C., Stote, R., Straub, J., Watanabe, M., Wiorkiewicz-Kuczera, J., Yin, D., and Karplus, M. (1998) All-Atom Empirical Potential for Molecular Modeling and Dynamics Studies of Proteins. *J. Phys. Chem. B 102*, 3586−3616.
(60) Darnell, S. J., LeGault, L., and Mitchell, J. C. (2008) KFC Server: interactive forecasting of protein interaction hot spots. *Nucleic Acids Res. 36*, W265−W269.
(61) Humphrey, W., Dalke, A., and Schulten, K. (1996) VMD: visual molecular dynamics. *J. Mol. Graphics 14*, 33−38.
(62) Sheffield, P., Garrard, S., and Derewenda, Z. (1999) Overcoming expression and purification problems of RhoGDI using a family of "parallel" expression vectors. *Protein Expression Purif. 15*, 34−39.
(63) Beauchamp, C., and Fridovich, I. (1971) Superoxide dismutase: improved assays and an assay applicable to acrylamide gels. *Anal. Biochem. 44*, 276−287.
(64) Banerjee, V., and Das, K. P. (2012) Modulation of pathway of insulin fibrillation by a small molecule helix inducer 2,2,2-trifluoroethanol. *Colloids Surf., B 92*, 142−150.

DOI: 10.1021/acschemneuro.6b00227
ACS Chem. Neurosci. 2016, 7, 1595−1606